

Article

A Case Study of the Integration of Ground-Based and Drone-Based Ground-Penetrating Radar (GPR) for an Archaeological Survey in Hulata (Israel): Advancements, Challenges, and Applications

Michael Frid¹ and Vladimir Frid^{2,*} ¹ Geo-Scope Ltd., Rosmarine 17, Beer Sheva 8465041, Israel; geoscopegpr@gmail.com² Civil Engineering Department, Sami Shamoon College of Engineering, Jabotinsky 84, Ashdod 77245, Israel

* Correspondence: vladimirf@ac.sce.ac.il

Abstract: This study delves into the fusion of ground-based and drone-based ground-penetrating radar (GPR) technologies in archaeological exploration. Set against the backdrop of the Hulata solar panel construction site in Israel, the research confronts daunting obstacles such as clayey soil, accurate detection of small objects, and the imperative of timely reporting crucial for construction management. The drone-based GPR, a testament to technological innovation, showcases remarkable adaptability to challenging terrains, dispelling doubts about electromagnetic wave decay in clayey soil. Methodologically, the study employs detailed orthophoto mapping and grid-type surveys. The correlation of the results significantly bolsters the reliability of archaeological discoveries, uncovering scattered artifacts buried approximately 1–1.5 m below the surface. Meticulous excavations validate the geophysical surveys, affirming the presence of structures constructed from boulders. The application at the Hulata site validates the adaptability of drone-based GPR in challenging terrains. It provides a swift, cost-effective, and minimally invasive alternative to traditional excavation techniques, thereby transforming the field of archaeology.

Keywords: ground-based GPR; drone-based GPR; archeological survey

Citation: Frid, M.; Frid, V. A Case Study of the Integration of Ground-Based and Drone-Based Ground-Penetrating Radar (GPR) for an Archaeological Survey in Hulata (Israel): Advancements, Challenges, and Applications. *Appl. Sci.* **2024**, *14*, 4280. <https://doi.org/10.3390/app14104280>

Academic Editor: Atsushi Mase

Received: 18 April 2024

Revised: 10 May 2024

Accepted: 14 May 2024

Published: 18 May 2024



Copyright: © 2024 by the authors. Licensee MDPI, Basel, Switzerland. This article is an open access article distributed under the terms and conditions of the Creative Commons Attribution (CC BY) license (<https://creativecommons.org/licenses/by/4.0/>).

1. Introduction

1.1. State of the Art

Ground-penetrating radar (GPR) plays a crucial role in archaeological exploration by providing a non-invasive understanding of subsurface characteristics [1–6]. Within archaeological research, site preservation, and cultural heritage conservation efforts, the prevalence of the GPR methodology has steadily increased over time. This rise can be attributed to several key factors: (a) their efficiency, utility, and cost-effectiveness render them invaluable tools for archaeological investigation and cultural heritage preservation, thereby minimizing excavation efforts and decreasing human energy expenditure; (b) they provide non-invasive and non-destructive approaches to site exploration, ensuring the conservation of investigated areas; (c) they allow for precise determination of the location of buried archaeological artifacts; and (d) by integrating with other disciplines, they facilitate the reconstruction of a site's history [6–10].

The utilization of a comprehensive methodology, integrating geophysical techniques (including ground-based GPR, remote aerial, and satellite imagery) along with archaeological inquiries at the Bronze Age site of Sissi on Crete, was detailed in [11]. The study revealed that conducting thorough geophysical surveys offers a more comprehensive understanding of unexcavated or partially excavated layouts. Barilaro et al. [12] used GPR to detect underground voids beneath the St. Sebastiano church in Catania (Sicily). They showed that GPR enabled their successful revealing. Barone et al. [10] demonstrated that GPR

allowed the identification of buried structures' positions, depths, and dimensions. It further facilitated the assessment of the foundation geometry and its structural integrity. The comprehensive field campaign confirmed the effectiveness of applying GPR with 200 and 400 MHz antennae [13]. It was shown that the anomalies observed by GPR corresponded to fire-hearth structures, wooden artifacts, tree roots, and rocky bodies, such as speleothems, boulders, and bedrock.

Observations indicate that the persistent application of conventional ground-penetrating radar (GPR) acquisition and processing methodologies is imperative for investigating subterranean cultural artifacts. Nevertheless, there is a strong emphasis on adopting innovative approaches for data acquisition, post-processing, and interpretation [1]. One advantage is using a multi-antenna array for large study areas and a pseudo-3D methodology based on collecting several parallel lines [3,4,8]. Several successful applications of such methods were demonstrated in [3]. Another way to improve the quality of GPR studies is by integrating them with other geophysical techniques. For example, the applicability of magnetic, ERT, and electromagnetic induction methods was highly prospective in the integration with GPR [2]. The preliminary results, which showed the existence of Early Bronze Age (c. 2600–2400 BC) buildings and pottery in the Syrian Middle-Euphrates valley [14], motivated the application of GPR, which revealed the existence of unknown buildings on the streets and the enclosure wall of the city. Another example showcasing the successful use of GPR was highlighted in [15], which revealed traces of ancient human activity during the Stone and Bronze Age periods at the Asaviec settlement site in Northern Belarus.

The procedures for the application of the magnetic and resistivity methods were reviewed in detail in [16,17]. It was noted that three-dimensional and virtual-reality models have become common, and the integration of the results of several methods is quite desirable [18]. An example of the successful combination of GPR with magnetic mapping and magnetic susceptibility measurements was presented in [19], which has proven effective in identifying concealed archaeological structures. This integrated approach was beneficial for delineating the spatial arrangement of buried remains, characterizing the geometry of anthropogenic settlements, and obtaining detailed insights into various building materials' composition and manufacturing processes. An attempt was made to integrate the fluxgate gradiometer and electromagnetic induction methods with GPR in the prospection of Bronze Age circular ditches in the western part of Belgium [20]. It was shown that GPR allowed the detection of a concentric and a single monument, while the fluxgate gradiometer and electromagnetic induction methods were unsuccessful in revealing the ditches.

A comprehensive study of the sedimentary conditions typical of archeological projects was performed in [5]. It was shown that GPR finds its most relevant applications in geoarchaeological contexts within fluvial, beach, and associated aeolian environments. These areas, rich in archaeological sites, prove ideal for various GPR methods. Caves pose more significant challenges due to being characterized by thick floor sequences of thin stratigraphic units, necessitating low-frequency antennae for depth penetration but at the cost of lower resolution. Promising prospects lie ahead for GPR in lakes, swamps, and bogs, offering good depth penetration despite potential difficulties in terms of access and collection. Urban environments present the most complexity due to anthropogenic stratigraphy, requiring detailed profile analysis in a closely spaced grid for interpretation, with amplitude slice-maps only understood at subsequent stages.

Airborne ground-penetrating radar (GPR) is an advanced technology employing electromagnetic waves to delve into the subsurface and capture intricate geological data [21]. Unlike conventional ground-based GPR, drone-based GPR presents numerous advantages [22]. Equipped with GPR sensors, unmanned aerial vehicles (UAVs) can swiftly and non-invasively cover extensive areas, providing a comprehensive three- or even four-dimensional view of subsurface boundaries and their geotechnical characteristics, thus achieving enhanced spatial resolution [23]. Using real-time kinematic (RTK) GPS positioning facilitates the replication of precise survey paths [24]. It is incorporated with signal processing techniques like cross-correlation-based background subtraction and interference

suppression, ensuring the accurate identification of subsurface targets [25,26]. Drone-borne GPR enables the mapping of geotechnical properties such as the soil moisture [27] and field-scale soil electrical conductivity [28].

This technology proves invaluable in areas with limited accessibility, such as hill slopes prone to landslides or regions affected by colliery waste. Ruols et al. [29] effectively captured a significant 3D dataset using drone-borne controlled-source electromagnetic (CSEM) systems over alpine glaciers, demonstrating the feasibility of obtaining detailed imagery of the immediate subsurface in challenging terrains. The utility of drone-mounted GPR in guiding and optimizing mining operations is showcased in [30]. By mounting two 120 MHz GPR antennas (RADARTEAM SWEDEN AB, Boden, Sweden) on a drone, they successfully mapped the structural discontinuities within local geological materials in a quarry excavation area in Falconara Albanese, Italy. This application underscores the adaptability of drone-based GPR for specific geological investigations.

Edemsky et al. [31] conducted experiments in challenging clay soils, identifying characteristic features in the upper subsurface environment using airborne GPR. However, they acknowledge the challenges of employing GPR in clayey soil, where electromagnetic waves rapidly decay [32]. Nonetheless, this challenge is surmountable, as Cheng et al. [33] demonstrated in their use of land-based GPR for mapping disturbed clayey layers in agricultural fields.

Nevertheless, employing GPR in clay-rich soils, where electromagnetic waves dissipate rapidly, poses a considerable challenge [33,34]. Our investigation directly addresses this challenge by optimizing the GPR performance in clayey landscapes—an essential undertaking given the predominantly clayey soil composition at the Hulata construction site in northern Israel. In so doing, it builds upon the groundwork laid by [31,32], pushing the boundaries of GPR's applicability in demanding environments.

In addition to the challenge of clayey soils, detecting small artificial objects (~0.3–0.5 m) buried underground is another significant obstacle in archaeological studies, as whether deciphering fragments of historical artifacts or identifying remnants of past structures, the intricate nature of these minor archaeological features necessitates advanced detection precision.

1.2. The Motivation for the Study: Archeological and Geological Features of the Site

This investigation was initiated due to the impending construction of solar panels within an area historically significant for agriculture and habitation spanning millennia, as evidenced by archaeological discoveries across diverse historical epochs, a practice commonly referred to as preventive archaeology [35,36]. In the dynamic setting of a construction site, the importance of prompt and accurate results is heightened due to time constraints. Any delays could result in significant financial losses and disruptions to the construction timeline. Therefore, engineers and archaeologists must address the challenge of providing rapid results. This involves optimizing the efficiency of data collection and streamlining the processing and interpretation of the acquired data.

1.3. Archeological and Geographical Aspects

The site is in the Hula Valley in the Upper Galilee region of northern Israel (Figure 1a). Hulata is a kibbutz with profound archaeological significance. The region has clayey soil, coupled with its proximity to perennial water sources such as the Jordan River (less than 1 km east) and the Hula swamps (1 km to the north).

The Hulata site is exemplified by the discovery of a sugar mill dating back to the Mamluk period. This is evidenced by the uncovered remains of a building with two rows of columns located approximately 400 m northeast of the Hulata solar panel construction site [36–38]. Additionally, north of the condemned area, excavation revealed a tomb from the Early Bronze Age, accompanied by pottery fragments indicative of the same era [36–41]. Notably, a pottery offering discovered at the site heightened the prospect of further ancient artifacts in the vicinity, necessitating an urgent and comprehensive inspection of approximately 40 dunams (1 dunam is equal to 1000 m²) to systematically

map the subterranean antiquities. The historical depth of Hulata, manifested in these archaeological findings, underscores the imperative of meticulous exploration to unveil and preserve its rich cultural heritage.

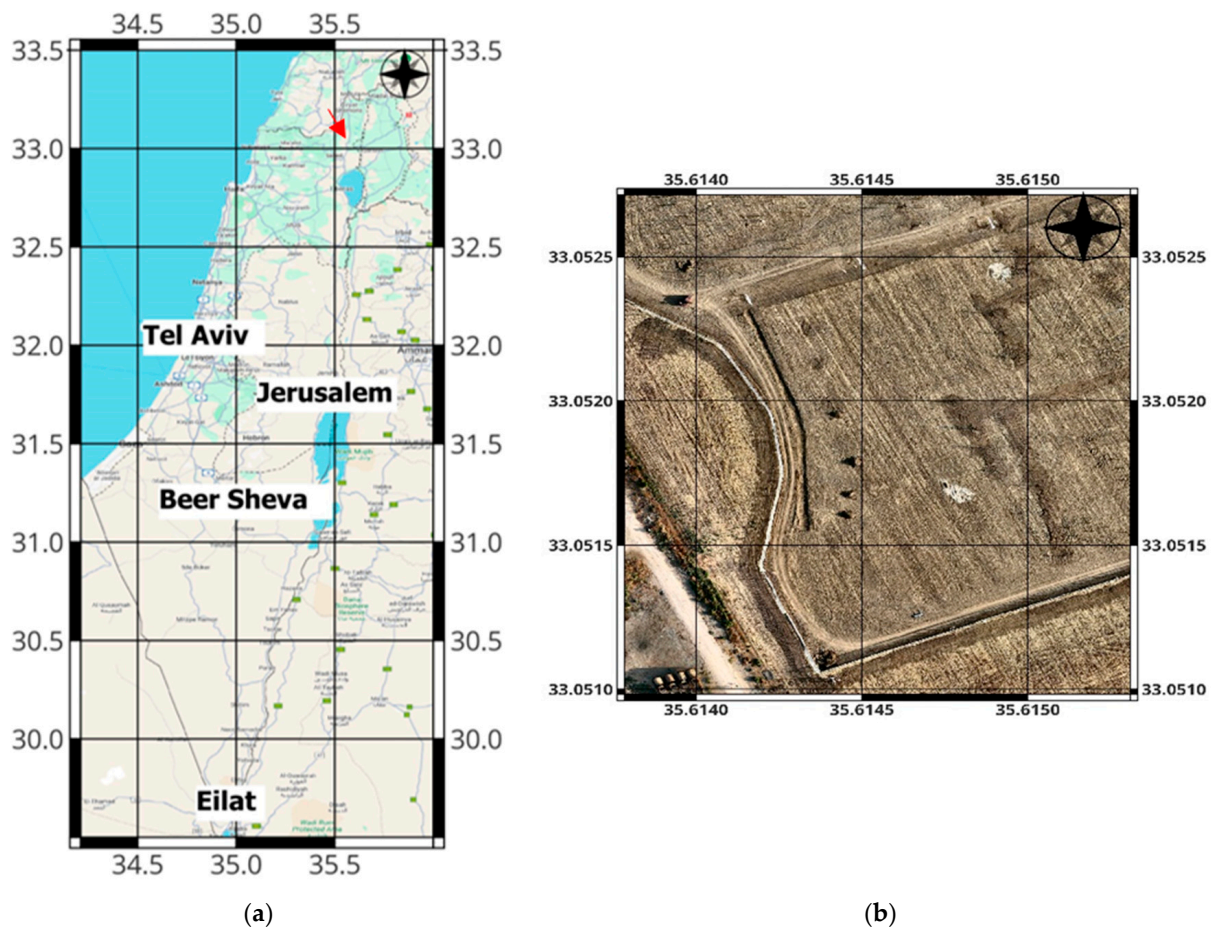


Figure 1. The location of the GPR survey. (a) The site's location under study is marked by the red arrow (zoom-out map). (b) The detailed orthophoto map of the surveyed area provides a high-resolution visual representation to complement the ground-penetrating radar (GPR) data for enhanced interpretation of the subsurface archaeological features.

Figure 1b presents a detailed orthophoto map, offering a high-resolution visual representation of the surveyed terrain.

1.4. Geological Features

Nestled in the heart of the Upper Galilee Valley, the Hulata solar panel construction site unfolds within the embrace of the modern geological landscape [42]. The site, located within the modern Bashan–Hula formation, rests atop a tapestry of Alluvium soil. This soil formation is predominantly characterized by a clayey-sand composition, a significant factor influencing the subsurface dynamics and challenging the efficacy of traditional surveying methods.

2. Methods and Tools

2.1. Components and Integration

Ground-based and drone-based GPR systems comprise several essential components, each playing a pivotal role in ensuring the accuracy and functionality of the technology. First and foremost, the core of this system is the GPR unit itself. The single-unit GPR includes the radar transmitter and receiver antennas, which emit electromagnetic waves

into the ground and capture the reflected signals. These antennas are crucial for collecting subsurface data and are typically chosen based on the specific application, considering factors like the desired penetration depth and resolution. The drone-based GPR is produced by Radar Systems Inc. (Radsys, Riga, Latvia), and the ground-based GPR is produced by Sensors & Software Inc. (from Radiodetection, Bristol, UK).

Integrating GPR technology with drones for archaeological surveys represents a synergistic union between aerial platforms and subsurface sensing capabilities. As seen in Figure 2a, the GPR unit is securely mounted onto the drone, situated underneath the drone, with the radar antennas facing downwards. This arrangement allows the drone to carry the GPR system while ensuring it maintains an optimal distance from the ground to capture data accurately. Additionally, RTK technology is integrated to provide georeferencing, enabling precise data mapping to specific geographical coordinates. Data synchronization between the DJI M300 drone (DJI, Shenzhen, China) and the GPR unit is meticulously maintained by the SkyHub computer (SPH Engineering, Riga, Latvia) to collect coherent and reliable information throughout the flight.

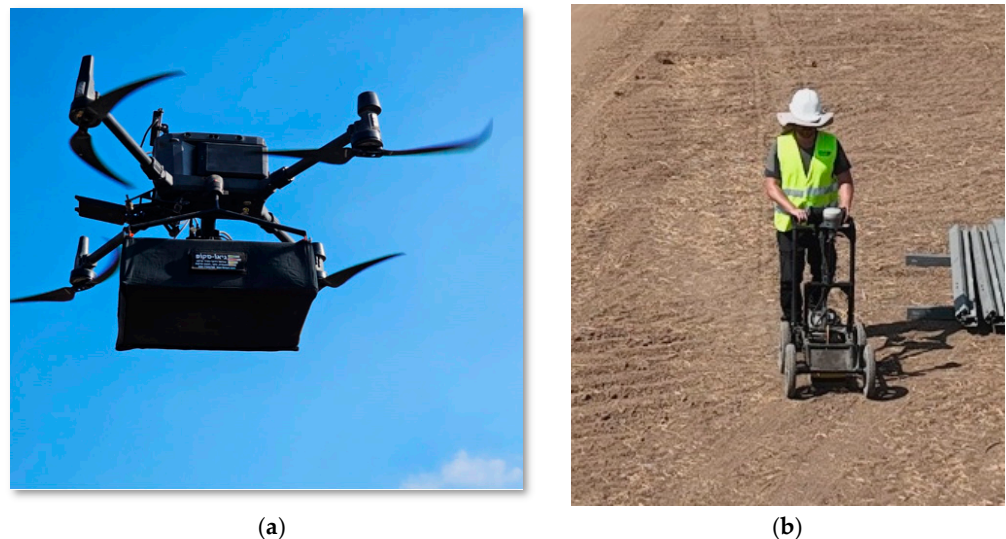


Figure 2. Two types of GPR instruments at the site under study. (a) A DJI M-300 drone with a GPR 500 MHz shielded dipole antenna is attached below. The SkyHub computer, which is positioned on the right side, is responsible for controlling the automatic flight operations. At the front of the drone, an altimeter measures the distance from the ground, maintaining a constant flight altitude. (b) An intelligent cart with a GPR 500 MHz shielded dipole antenna is attached in the middle. Both GPRs provide similar subsurface sensing capabilities up to 5 m below the surface.

Integrating GPR technology with drones for archaeological surveys represents a synergistic union between aerial platforms and subsurface sensing capabilities. As seen in Figure 2a, the GPR unit is securely mounted onto the drone, situated underneath the drone, with the radar antennas facing downwards.

Several key specifications must be considered to achieve optimal performance in such integration. The choice of GPR frequency is paramount, as it directly affects the penetration depth and the subsurface data resolution. Lower frequencies offer greater depth penetration but may sacrifice resolution, while higher frequencies provide finer details at shallower depths. The selection of the appropriate frequency band depends on the specific research objectives and the characteristics of the archaeological site. In the case of the Hulata archeological site, previous exploratory excavations performed by the Israel Antiquities Authority (IAA) [41] in the area brought up findings that indicated that the antiquities in the region are found up to a maximum depth of 2 m from the surface. Therefore, the chosen GPR central frequency was set to 500 MHz, with a built-in 500A antenna, 100 ns time range, and 512 samples per scan.

Furthermore, the drone’s payload capacity and flight time are critical factors determining the system’s overall usability. A well-balanced drone with sufficient payload capacity ensures the GPR unit can be mounted securely without compromising the flight stability, and longer flight times allow for extended data collection periods, which is essential for comprehensively covering large archaeological areas. Additionally, the data-processing capabilities of the drone, or the capacity to transmit data to a ground station for processing, influence the real-time utility of the system and the speed at which results can be obtained during an archaeological survey.

The ground-based GPR’s (Figure 2b) central frequency is the same as for the drone-based GPR (500 MHz), with a 100 ns time range and the dynamic option for the number of scans that ensures the optimal sample number per scan (usually between 8 and 16 stacks). The instrument was equipped with a GPS antenna with a license for the RTK technology integrated to provide accurate georeferencing.

2.2. Data Acquisition

2.2.1. The Survey Parameters

Designing an appropriate GPR survey grid pattern is crucial for data acquisition. Several factors come into play when deciding on the grid layout: spatial resolution, depth of penetration, the maximum exposed area, etc. Figure 3 shows the scheme for calculating the GPR parameters.

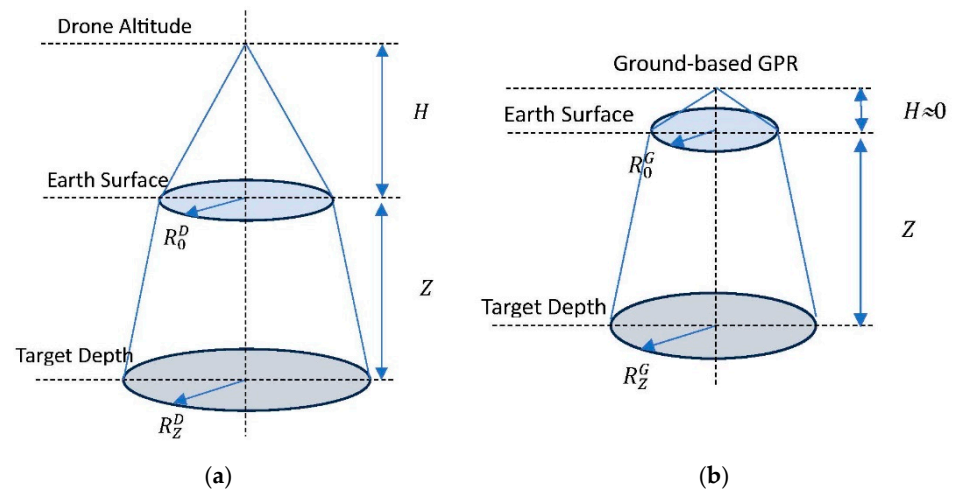


Figure 3. The scheme for calculating the GPR parameters: (a) drone-based GPR, and (b) land-based GPR.

Following [43–46], the general expression for the radius R_0 of the maximum exposure area under the GPR center on the Earth’s surface can be calculated as a function of the GPR altitude above the Earth’s surface H , the center frequency of GPR antenna f , and dielectric permittivity of the medium ϵ_a as follows:

$$R_0 = \frac{0.075}{f\sqrt{\epsilon_a}} + \sqrt{\frac{0.075H}{f\sqrt{\epsilon_a}}} \tag{1}$$

The constant ‘0.075’ units, H , and f , are m/ns, m, and GHz, respectively. Since the value of the dielectric permittivity of air is equal to 1, Equation (1) can be simplified as follows:

$$R_0^D = \frac{0.075}{f} + \sqrt{\frac{0.075H}{f}} \tag{2}$$

where R_0^D is the radius of the maximum exposure area under the GPR center for drone-based GPR on the Earth's surface. Equation (2), used for the radius calculation for drone-based GPR, can be simplified for the case of ground-based GPR, taking into account the fact that the height of the GPR antennae above the ground surface, in this case, is negligibly small ($H \approx 0$) and hence can be neglected:

$$R_0^G = \frac{0.075}{f} \quad (3)$$

Estimating R_Z , that is, the radius of the maximum exposure area under the GPR center at depth Z , based on Equation (2) yields:

$$R_Z^D = \frac{0.075}{f} + \sqrt{\frac{0.075}{f} \left(\sqrt{H} + \sqrt{\frac{Z}{\sqrt{\epsilon_s}}} \right)} \quad (4)$$

And for the case of ground-based GPR based on Equation (3):

$$R_Z^G = \frac{0.075}{f} + \sqrt{\frac{0.075}{f} \sqrt{\frac{Z}{\sqrt{\epsilon_s}}}} \quad (5)$$

The depth of the desirable object Z and the maximum vertical resolution of the survey D_Z are critical factors affecting the quality of data collected by GPR [41–44]. Balancing the depth and resolution is an ongoing challenge, and it is essential to strike a harmonious equilibrium to obtain the most informative and high-quality data during the GPR survey. The vertical resolution (D_Z) and minimum size (A_{\min}) of detectable objects can be calculated as follows [33,43–46]:

$$D_Z = \frac{0.15}{f\sqrt{\epsilon_s}} \quad (6)$$

where the unit of the coefficient '0.15' is m/ns, and

$$A_{\min} = \begin{cases} (Z + H)/10, & \text{if } (Z + H)/10 > D_Z \\ \frac{0.075}{f\sqrt{\epsilon_s}}, & \text{if } (Z + H)/10 \leq D_Z \end{cases} \quad (7)$$

An additional necessary parameter for the linear objects' detection (e.g., a wall) is their diameter (wall width), which follows [41–44], usually estimated as 0.25–0.5 of the wavelength in the soil or, in a conservative estimation, 0.4 of the soil wavelength:

$$D = (0.25 \div 0.5) \frac{0.3}{f\sqrt{\epsilon_s}} \approx 0.4 \frac{0.3}{f\sqrt{\epsilon_s}} \quad (8)$$

As can be seen, the flight altitude affects the data accuracy (Equations (2), (4) and (7)) and hence must be optimized. Our experience shows that the flight altitude for small objects should be no more than 1 m above the Earth's surface. Similarly to ground-based GPR, while scanning for small objects, slow velocity scanning is preferable; therefore, the flight speed was set to 1 m/s. Considering the typical near-surface soil lithology (Section 1.3), the estimated value of dielectric permittivity ϵ_s was ~ 3 . This value was checked using the common for GPR measurements hyperbolic method.

Table 1 shows the values of the estimated parameters (Equations (4)–(8)) for both used GPR instruments, assuming that the altitude of the drone-based GPR is $H = 1$ m above the Earth's surface and the desirable maximal depth of measurements $Z = 2$ m.

Table 1. The values of the estimated GPR parameters.

Parameter Description	Eq.	Parameter Symbol	Drone-Based GPR, m	Ground-Based GPR, m
The radius of the maximum exposure area at the depth $Z = 2$ m	4, 5	R_Z^D R_Z^G	0.96	0.57
Vertical resolution	6	D_Z		0.17
The minimum size of a single detectable object at the depth $Z = 2$ m	7	A_{min}	0.3	0.2
The diameter of a linear object (wall width)	8	D	$(0.09-0.17) \approx 0.14$	

Analysis of Table 1 shows that both GPR instruments can be used for studying underground archeological objects at the site under study, the width of which is usually at least 0.3–0.5 m.

2.2.2. The Survey Parameters

The survey area depicted in Figure 4's orthophoto map underwent thorough scanning using land-based GPR (red grid) and drone-based GPR (blue grid). Extensive lines were established in the north–south and east–west directions using a grid-type survey strategy. The non-regular blue lines of the drone-based GPR mean the drone is arriving to charge and departing for the next survey step. The maximum depth for the subsurface investigation was consistently set at 5 m below the surface in both methodologies. The survey velocity maintained a uniform rate of approximately 1 m per second for the ground- and drone-based GPR scans. Precise real-time kinematic (RTK) measurements of the surveying process were meticulously recorded, enhancing the accuracy and reliability of the acquired data. The distance between nearby lines was 3 and 2 m for land-based and drone-based GPR, respectively. The overall area studied by each instrument was 8500 m². This mapping initiative was critical to our multidimensional approach, augmenting the GPR data to enhance the accuracy and interpretation of the subsurface archaeological features within the construction site.

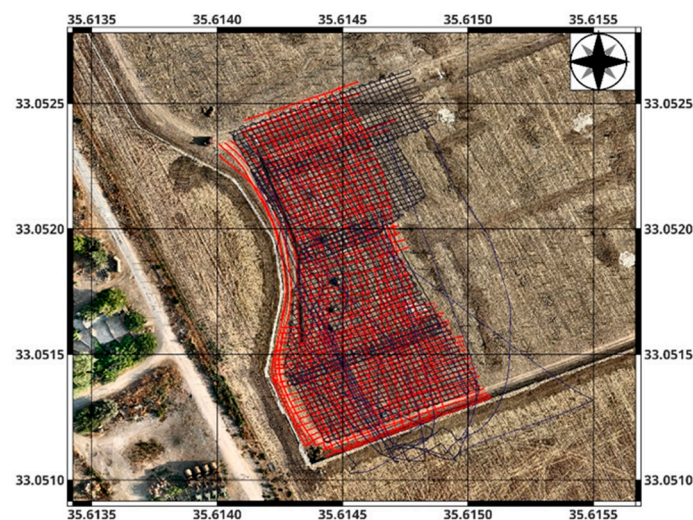


Figure 4. Two grids of GPR surveys. The red grid is for ground-based GPR, and the blue grid is for drone-based GPR.

2.3. Data Processing

The signal-processing stage is crucial when interpreting GPR data. With an increasing depth, the radar reflection energy diminishes rapidly within the medium, resulting in the

target's amplitude being smaller than the background signals. The employed processing techniques aimed at accentuating faint signals and discerning deep underground targets.

Table 2 shows the filters applied to the raw GPR data collected by both instruments to enhance the signal-to-noise (SNR) ratio.

Table 2. The list of filters applied to the raw GPR data.

	Filter Type	Drone-Based GPR	Ground-Based GPR
1	Data Editing	+	
2	'Dewow'	+	+
3	Static Correction	+	+
4	Background Removal	+	+
5	X-Interpolation by GPS Coordinates	+	+
6	Median Filter	+	+
7	Automatic Gain Control	+	+
8	Stolt (F-K) Method	+	+

A comparison of the lists of filters reveals that they were identical except for the data-editing filter. Data editing utilizing GeoHammer Software (v.1.1.10) (SPH Engineering, Riga, Latvia) involves removing the drone trajectory segments between adjacent lines and the flight data from the ground station to the survey's starting point and from the survey's final point to the drone's base station. This procedure enables us to eliminate inaccurate GPR data characterized by a heightened amplitude resulting from drone maneuvers and data captured during flights with higher velocity from and to the ground station. Breaking down a 'large' source file into multiple lines streamlines the data-processing procedure and diminishes the time required for data processing. Figure 5 shows the flight scheme before (a) and after (b) the GeoHammer application.

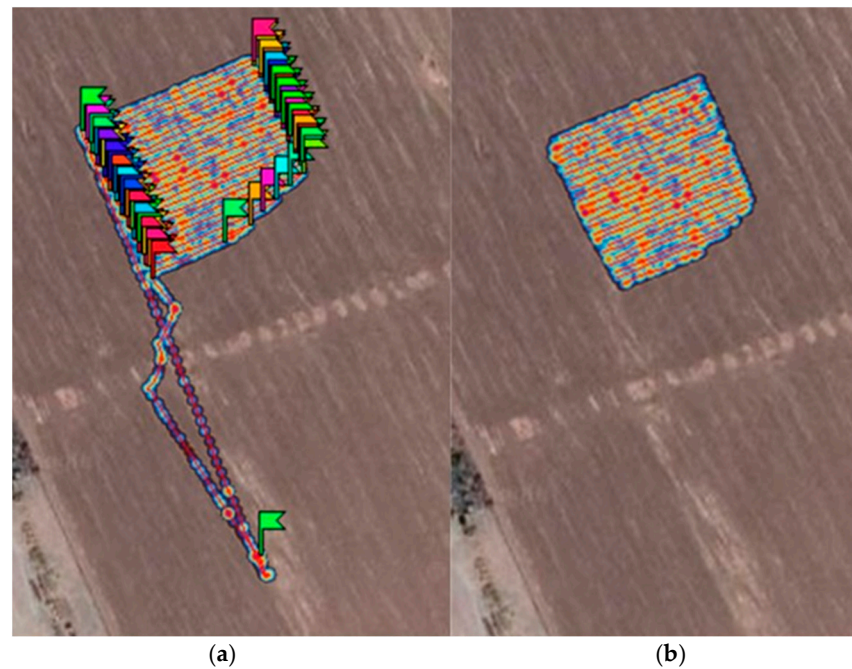


Figure 5. The part of the drone flight program before (a) and after (b) the application of GeoHammer software.

The processing of the data collected by drone-based GPR was continued using Prism 2 software (RADAR Systems Inc., Riga, Latvia), while those by ground-based—using the software REFLEXW [47].

3. Results

Figure 6 displays zoomed-in fragments of the radargrams extracted from a drone-based (a) and ground-based (b) GPR survey line. The X and Y axes represent the line distance along the Earth's surface and the measurement depth in meters, respectively. A discernible change between two geological layers is evident approximately 1 m below the surface, demarcated by a black dashed line. The upper soil exhibits a softer composition, characterized by the faster decay of the electromagnetic waves, resulting in a low-amplitude representation depicted with weak and blurred colors. Below this depth, a pronounced amplification reveals a denser layer. Several heterogeneous anomalies are observed within the upper soil layer, particularly around 0.3 m deep, indicating irregularities near the surface. These anomalies suggest that the terrain may not have been uniformly flat and might have undergone alterations for construction purposes, leading to localized soil 'pockets' near the surface, as delineated by a yellow dashed line. In the lower soil layer, distinct changes in the horizontal electromagnetic phases are noted at approximately 62–63 m of the profile length, accompanied by heightened amplification. This pattern suggests the presence of objects composed of stiffer materials, likely artificial structures such as archaeological walls made of limestone boulders, marked by a light blue dashed line. Note that the corresponding structural elements on both radargrams are emphasized by circles and dashed arrows.

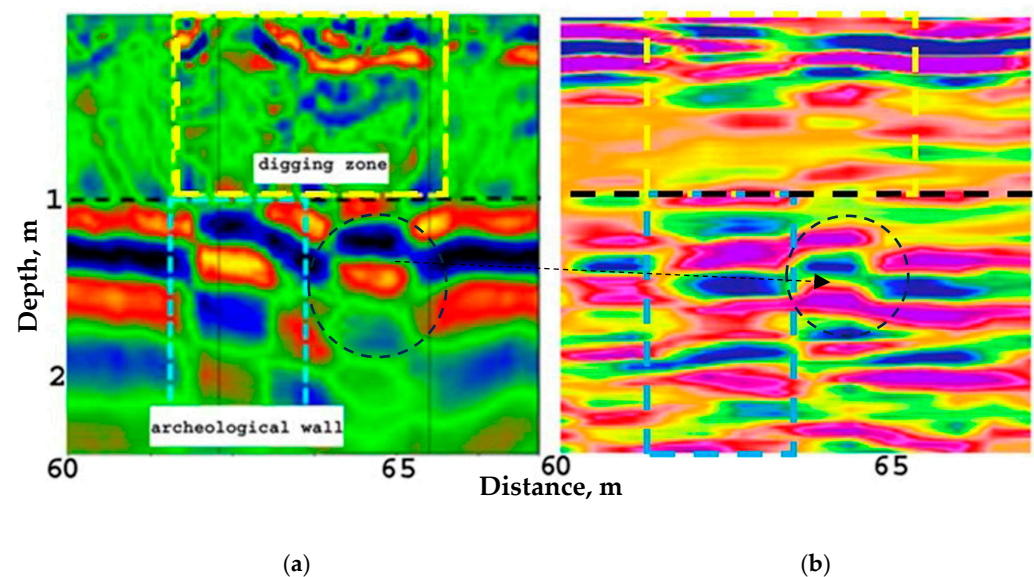


Figure 6. Two radargram excerpts from a drone-based GPR survey (a) and ground-based GPR (b) lines showcase a distinct geological transition approximately 1 m below the surface. A black dashed line demarcates the boundary between two soil layers. The upper soil layer exhibits anomalies at around 0.3 m, suggesting irregular terrain (the yellow dashed lines). In comparison, the lower layer reveals changes in the electromagnetic phases at 62–64, indicative of potential artificial structures, possibly archaeological walls made of limestone boulders (the light blue dashed lines). The corresponding structural elements on both radargrams are emphasized by circles and dashed arrows.

Figure 7 presents the mapped archaeological finding, distinguishing between ground-based GPR (small dots) and drone-based GPR (large dots). The color-coded scheme signifies different surveying groups corresponding to the direction of the GPR lines. For instance, the prominent red dots in the northern region represent drone-based GPR findings from east–west (EW) direction flights, while the significant green dots denote drone-based GPR

findings from north–south (NS) direction flights. The determined correspondence between the ground- and drone-based measurements implies that the recorded anomalies are consistent across both the ground and drone measurements and the NS and EW directions. Only those found that were recorded by at least three independent observations were considered important archaeological targets to enhance confidence in the archaeological significance of the subsurface features.

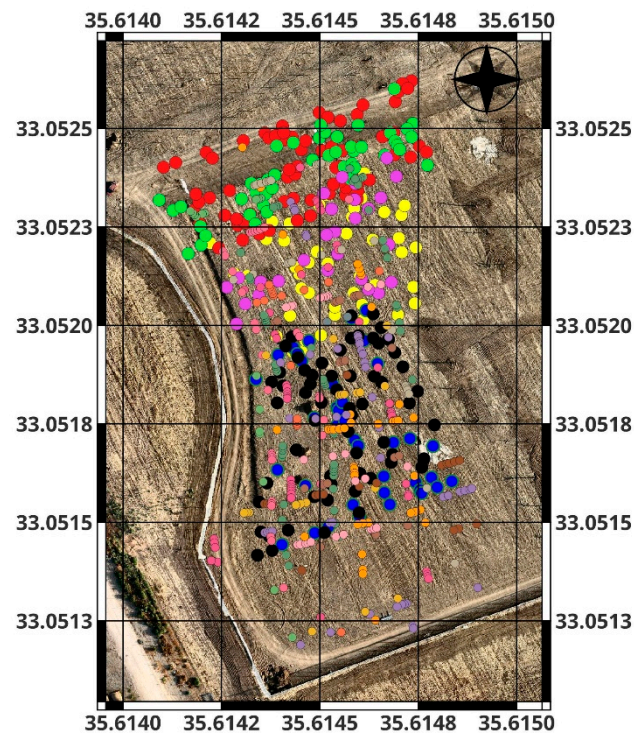


Figure 7. The map of suspected archaeological findings at the Hulata solar panel construction site indicates ground-based GPR discoveries (small dots) and drone-based GPR findings (large dots). Colors correspond to different surveying groups based on the direction of the GPR lines.

Figure 8 shows the numerical mapping of the overlapping findings. The locations and shapes of the findings are irregular and randomly scattered across the site. Such a feature of the outcomes suggests the relation to the Early Bronze Age. This era was characterized by structures crafted from irregularly broken limestone and sandstone boulders intricately assembled into wall-like structures, as highlighted in the preceding introduction. The unique scattering pattern observed in this mapping aligns with the archaeological understanding of construction practices during the Early Bronze Age in the Hulata region.

This study's results (Figure 8) show that the target archaeological artifacts are scattered underground throughout the entire site, typically at depths of approximately 1–2 m. The Archaeological Authority of Israel (AAI) conducted precise experiential excavations at several suspected points of interest within the site area and a few attempts outside the GPR-investigated area. Two examples of shallow and short trenches, the photos of which are incorporated into Figure 9, were dug to a depth of 2 m. The archaeological findings align with the geophysical survey results, indicating that archaeological artifacts are located at depths estimated by the GPR findings. These artifacts consist of randomly shaped structures made mainly of boulders, with a density higher than the surrounding soil. This correlation reinforces the accuracy and reliability of our geophysical survey in identifying archaeological features within the Hulata solar panel construction site.

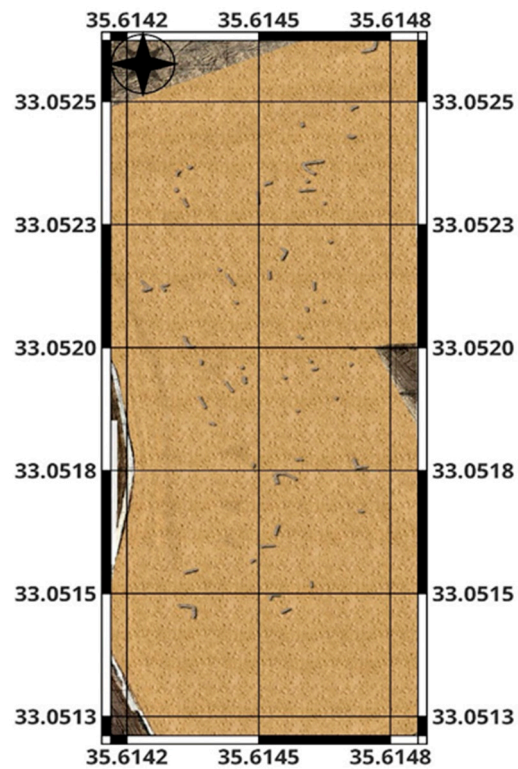


Figure 8. Numerically mapped locations of overlapping ground-based and drone-based GPR findings, presenting potential archaeological artificial objects, likely walls or concentrations of pottery. The irregular scattering pattern suggests a connection to the Early Bronze Age construction practices observed in the Hulata region, characterized by structures crafted from irregularly broken limestone and sandstone boulders.

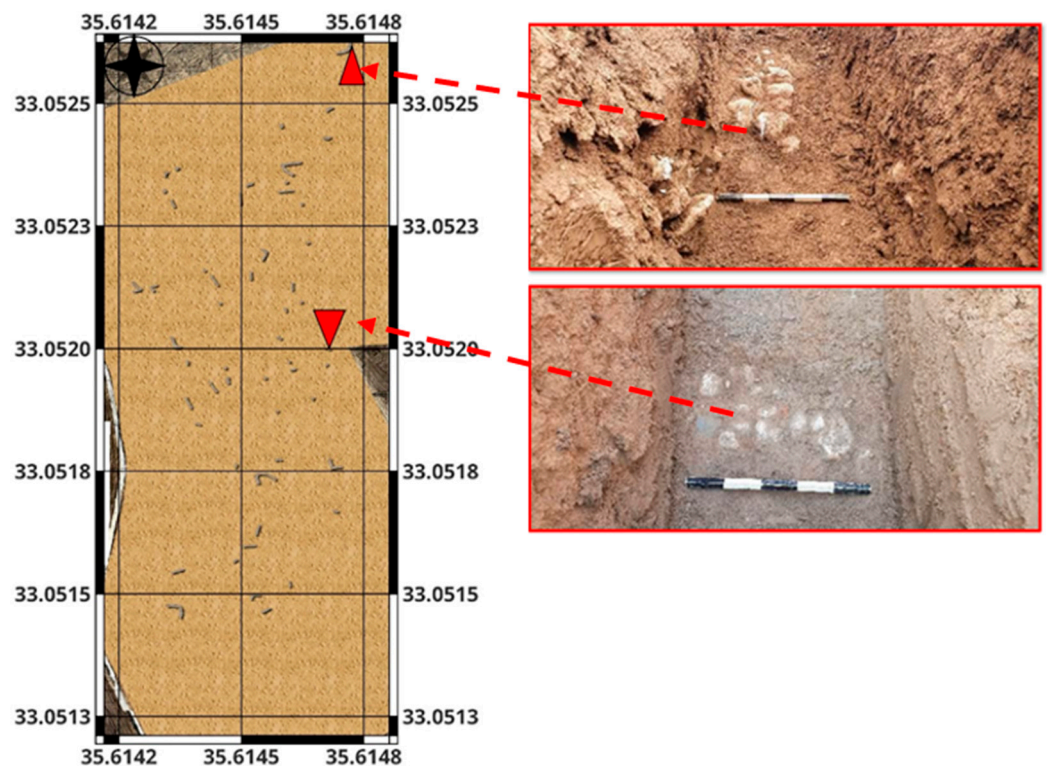


Figure 9. Excavation trenches and corresponding archaeological findings at the Hulata solar panel construction site.

4. Discussion

The use of ground-based and drone-based GPR has its advantages and disadvantages. For example, ground-based GPR data will, in principle, have higher reflection amplitudes because the antenna is closer to the ground. However, the data quality depends on slight surface morphology, mainly when the GPR is used in agricultural environments. In addition, using ground-based GPR over a large area and grid is time-consuming. Significant efforts are required to maintain the grid parameters (e.g., the distance between nearby lines and their exact direction).

Drone-based GPR measurements employing RTK technology are less time-consuming and avoid issues with line positioning. Unlike ground-based GPR systems, the drone-based setup navigates without surface obstacles, facilitating a smoother and more precise scanning process. This is crucial for studies conducted over rugged terrains or unmanaged agricultural fields. Moreover, the drone's ability to fly over terrain and capture data without disruptions contributes to a more efficient and comprehensive subsurface mapping. Our study demonstrates that maintaining a relatively low flight altitude (1 m above the Earth's surface) results in a maximum exposure area at a depth of 2 m, which is twice that of ground-based GPR, while preserving the resolution of linear targets (refer to Table 1). However, the amplitude of the reflections is diminished in comparison to ground-based radargrams.

Combining two GPR methodologies yields overlapping outcomes, reinforcing the quality and dependability of archaeological discoveries. Moreover, the likelihood of uncovering significant findings is heightened by cross-referencing and validating data gathered via two distinct GPR measurement techniques. Another noteworthy outcome of our study is the effective use of drone-based GPR in clayey soil. The successful application in this challenging environment highlights the adaptability and reliability of drone-based GPR technology. This finding suggests that the methodology can be employed in other locations characterized by clayey soil, broadening the applicability of drone-based GPR in archaeological and geophysical investigations. Overall, the study reinforces GPR's standing as a fast, cost-effective, and dependable solution for archaeological subsurface surveys, with drone-based technology demonstrating particular promise in addressing challenging terrains.

5. Conclusions

1. This study employs and correlates ground-based and drone-based ground-penetrating radar (GPR) technologies. Integrating these two distinct GPR methods enhances the accuracy and effectiveness of archaeological surveys, ushering in a new approach for comprehensive subsurface mapping.
2. The effective utilization of drone-based GPR technology in clayey soil at the Hulata solar panel construction site showcases the versatility of drone-based technology in tackling demanding soil conditions and, hence, opens up new avenues for archaeological inquiries in regions where clayey soil was previously deemed a hindrance.
3. This study enhances the reliability and accuracy of subsurface mapping by independently deploying ground-based and drone-based GPR systems technologies and cross-referencing their findings.

Author Contributions: Conceptualization, M.F. and V.F.; methodology, M.F. and V.F.; software, M.F.; validation, M.F. and V.F.; formal analysis, M.F.; investigation, M.F. and V.F.; resources, V.F.; data curation, V.F.; writing—original draft preparation, M.F. and V.F.; writing—review and editing, M.F. and V.F.; visualization, M.F.; supervision, V.F.; project administration, M.F. All authors have read and agreed to the published version of the manuscript.

Funding: V.F. acknowledges the support from the European Union's Horizon 2020 research and innovation program under the Marie Skłodowska-Curie RISE project EffectFact, grant agreement no. 101008140.

Data Availability Statement: The original contributions presented in the study are included in the article, further inquiries can be directed to the corresponding author.

Conflicts of Interest: Author Michael Frid was employed by the company Geo-Scope Ltd. The remaining authors declare that the research was conducted in the absence of any commercial or financial relationships that could be construed as a potential conflict of interest.

References

1. Conyers, L.B.; Leckebusch, J. Geophysical Archaeology Research Agendas for the Future: Some Ground-Penetrating Radar Examples. *Archaeol. Prospect.* **2010**, *17*, 117–123. [[CrossRef](#)]
2. Pettinelli, E.; Barone, P.M.; Mattei, E.; Lauro, S.E. Radio wave techniques for non-destructive archaeological investigations. *Contemp. Phys.* **2011**, *52*, 121–130. [[CrossRef](#)]
3. Goodman, D.; Piro, S. *GPR Remote Sensing in Archaeology*; Springer: Berlin/Heidelberg, Germany, 2013. [[CrossRef](#)]
4. Novo, A. Ground-Penetrating Radar (GPR). In *Good Practice in Archaeological Diagnostics; Natural Science in Archaeology*; Corsi, C., Slapšak, B., Vermeulen, F., Eds.; Springer International Publishing: Cham, Switzerland, 2013. [[CrossRef](#)]
5. Conyers, L.B. *Ground-Penetrating Radar for Geoarchaeology*; John Wiley & Sons, Ltd.: Hoboken, NJ, USA, 2016.
6. Martorana, R.; Capizzi, P.; Pisciotta, A.; Scudero, S.; Bottari, C. An Overview of Geophysical Techniques and Their Potential Suitability for Archaeological Studies. *Heritage* **2023**, *6*, 2886–2927. [[CrossRef](#)]
7. Batayneh, A.T. Archaeogeophysics—archaeological prospection—A mini review. *J. King Saud-Univ. Sci.* **2011**, *23*, 83–89. [[CrossRef](#)]
8. Martinho, E.; Dionísio, A. A review of the main geophysical techniques used for non-destructive evaluation in cultural built heritage. *J. Geophys. Eng.* **2014**, *11*, 053001. [[CrossRef](#)]
9. Deiana, R.; Leucci, G.; Martorana, R. New perspectives on geophysics for archaeology: A special issue. *Surv. Geophys.* **2018**, *39*, 1035–1038. [[CrossRef](#)]
10. Barone, P.M.; Graziano, F.; Pettinelli, E.; Ginanni Corradini, R.G. Ground-penetrating Radar Investigations into the Construction Techniques of the Concordia Temple (Agrigento, Sicily, Italy). *Archaeol. Prospect.* **2007**, *14*, 47–59. [[CrossRef](#)]
11. Driessen, J.; Sarris, A. Archaeology and Geophysics in Tandem on Crete. *J. Field Archaeol.* **2020**, *45*, 571–587. [[CrossRef](#)]
12. Barilaro, D.; Branca, C.; Gresta, S.; Imposa, S.; Leone, A.; Majolino, D. Ground penetrating radar (G.P.R.) surveys applied to the research of crypts in San Sebastiano’s church in Catania (Sicily). *J. Cult. Herit.* **2007**, *8*, 73–76. [[CrossRef](#)]
13. Porsani, J.L.; de Matos Jangelme, G.; Kipnis, R. GPR survey at Lapa do Santo archaeological site, Lagoa Santa karstic region, Minas Gerais state, Brazil. *J. Archaeol. Sci.* **2010**, *37*, 1141–1148. [[CrossRef](#)]
14. Novo, A.; Solla, M.; Fenollós, J.-L.M.; Lorenzo, H. Searching for the remains of an Early Bronze Age city at Tell Qubr Abu al-’Atiq (Syria) through archaeological investigations and GPR imaging. *J. Cult. Herit.* **2014**, *15*, 575–579. [[CrossRef](#)]
15. Tšugai-Tsyrułnikova, A.; Charniauski, M.; Khrustaleva, I.; Plado, J.; Kriiska, A. Ground-penetrating radar investigations of the ASAVIEC 2 archaeological site, Northern Belarus. *Geoarchaeology* **2022**, *37*, 682–693. [[CrossRef](#)]
16. Bevan, B.W.; Smekalova, T.N. Magnetic Exploration of Archaeological Sites. In *Good Practice in Archaeological Diagnostics; Natural Science in Archaeology*; Corsi, C., Slapšak, B., Vermeulen, F., Eds.; Springer International Publishing: Cham, Switzerland, 2013. [[CrossRef](#)]
17. Monfort, C.C. Earth Resistance Survey: A Mature Archaeological Geophysics Method for Archaeology. In *Good Practice in Archaeological Diagnostics; Natural Science in Archaeology*; Corsi, C., Slapšak, B., Vermeulen, F., Eds.; Springer International Publishing: Cham, Switzerland, 2013. [[CrossRef](#)]
18. Ronchi, D.; Limongiello, M.; Demetrescu, E.; Ferdani, D. Multispectral UAV Data and GPR Survey for Archeological Anomaly Detection Supporting 3D Reconstruction. *Sensors* **2023**, *23*, 2769. [[CrossRef](#)] [[PubMed](#)]
19. Chianese, D.; D’Emilio, M.; Di Salvia, S.; Lapenna, V.; Ragosta, M.; Rizzo, E. Magnetic mapping, ground penetrating radar surveys and magnetic susceptibility measurements for the study of the archaeological site of Serra di Vaglio (Southern Italy). *J. Archaeol. Sci.* **2004**, *31*, 633–643. [[CrossRef](#)]
20. Verdonck, L.; Simpson, D.; Cornelis, W.M.; Plyson, A.; Bourgeois, J.; Docter, R.; Van Meirverne, M. Ground-penetrating Radar Survey over Bronze Age Circular Monuments on a Sandy Soil, Complemented with Electromagnetic Induction and Fluxgate Gradiometer Data. *Archaeol. Prospect.* **2009**, *16*, 193–202. [[CrossRef](#)]
21. Zayed, T.; Dawood, T.; Abouhamad, M.; Alsharqawi, M. Special Issue “Ground Penetrating Radar (GPR) Applications in Civil Infrastructure Systems”. *Remote Sens.* **2022**, *14*, 5682. [[CrossRef](#)]
22. Altdorff, D.; Schliffke, N.; Riedel, M.; Schmidt, V.; van der Kruk, J.; Vereecken, H.; Becken, M. UAV-borne electromagnetic induction and ground-penetrating radar measurements: A feasibility test. *Water Resour. Res.* **2014**, *42*, W11403.
23. Eröss, R.; Stoll, J.B.; Bergers, R.; Tezkan, B. Three-component VLF using an unmanned aerial system as sensor platform. *First Break* **2013**, *31*. [[CrossRef](#)]
24. Booth, A.D.; Koylass, T.M. Drone-mounted ground-penetrating radar surveying: Flight-height considerations for diffraction-based velocity analysis. *Geophysics* **2022**, *87*, WB69–WB79. [[CrossRef](#)]
25. Shin, Y.H.; Shin, S.Y.; Rastiveis, H.; Cheng, Y.T.; Zhou, T.; Liu, J.; Habib, A. UAV-Based Remote Sensing for Detection and Visualization of Partially-Exposed Underground Structures in Complex Archaeological Sites. *Remote Sens.* **2023**, *15*, 1876. [[CrossRef](#)]
26. Wu, S.; Wang, L.; Zeng, X.; Wang, F.; Liang, Z.; Ye, H. UAV-Mounted GPR for Object Detection Based on Cross-Correlation Background Subtraction Method. *Remote Sens.* **2022**, *14*, 5132. [[CrossRef](#)]

27. Wu, K.; Rodriguez, G.A.; Zajc, M.; Jacquemin, E.; Clément, M.; De Coster, A.; Lambot, S. A new drone-borne GPR for soil moisture mapping. *Remote Sens. Environ.* **2019**, *235*, 111456. [[CrossRef](#)]
28. Wu, K.; Lambot, S. 2022 Analysis of Low-Frequency Drone-Borne GPR for Root-Zone Soil Electrical Conductivity Characterization. *IEEE Trans. Geosci. Remote Sens.* **2022**, *60*, 2006213. [[CrossRef](#)]
29. Ruols, B.; Baron, L.; Irving, J. High-density 3D and 4D GPR data acquisitions over alpine glaciers using a newly developed drone-based system (No. EGU23-9619). In Proceedings of the EGU General Assembly 2023, Vienna, Austria, 24–28 April 2023.
30. Saponaro, A.; Dipierro, G.; Cannella, E.; Panarese, A.; Galiano, A.M.; Massaro, A. A UAV-GPR Fusion Approach for the Characterization of a Quarry Excavation Area in Falconara Albanese, Southern Italy. *Drones* **2021**, *5*, 40. [[CrossRef](#)]
31. Edemsky, D.; Popov, A.; Prokopovich, I.; Garbatsevich, V. Airborne ground penetrating radar, field test. *Remote Sens.* **2021**, *13*, 667. [[CrossRef](#)]
32. Daniels, D. *Ground Penetrating Radar*; The Institute of Electrical Engineers: London, UK, 2004.
33. Cheng, Q.; Su, Q.; Binley, A.; Liu, J.; Zhang, Z.; Chen, X. Estimation of surface soil moisture by a multi-elevation UAV-based ground penetrating radar. *Water Resour. Res.* **2023**, *59*, e2022WR032621. [[CrossRef](#)]
34. Van Dongen, A.; Eeckhout, P.; Lo Buglio, D. Crossed Experimentations of Low-Altitude Surveys for the Detection of Buried Structures. *Int. Arch. Photogramm. Remote Sens. Spat. Inf. Sci.* **2022**, *46*, 505–512. [[CrossRef](#)]
35. Paez-Rezende, L.; Hulin, G. A Combined Approach Using GPR and Trial Trenches in Cherbourg for Archaeological Evaluation. *ArcheoSciences* **2021**, *45*, 101–103. [[CrossRef](#)]
36. Novaković, P.; Horňák, M.; Pia Guermami, M.; Stäuble, H.; Depaep, P.; Demoule, J.-P. Recent Developments in Preventive Archaeology in Europe. In Proceedings of the 22nd EAA Meeting in Vilnius, Vilnius, Lithuania, 31 August–4 September 2016.
37. Biran, A. Yesud Hama'ala. In *The New Encyclopedia of Archaeological Excavations in the Holy Land*; Israel Exploration Society & Carta: Jerusalem, Israel, 1993; Volume 4, 1510p.
38. Biran, A.; Shoham, Y. Remains of a Synagogue and of a Sugar Installation at Yesud Hama'alah. *Eretz-Isr. Archaeol. Hist. Geogr. Stud.* **1987**, *19*, 199–207. (In Hebrew)
39. Biran, A.; Urman, D. Yesud Hama'ala, Synagogue—1982–1983. *Excav. Surv. Isr.* **1983**, *2*, 110–111. (In Hebrew)
40. Berger, U.; Peterson, J.; Byrne, Y. Yesod HaMa'ala. *Archeology News (Hadashot Arkheologiyot): Excavations and Surveys in Israel*. Final Report 12.08.21. 2021, Volume 133, (In Hebrew). Available online: <https://www.jstor.org/stable/10.2307/27131476> (accessed on 1 January 2023).
41. Berger, U. Yesod HaMa'ala. *Archeology News (Hadashot Arkheologiyot): Excavations and Surveys in Israel*. Preliminary Report 16.10.17. 2017, Volume 129, (In Hebrew). Available online: <http://www.jstor.com/stable/26693614> (accessed on 1 January 2023).
42. Sneh, A.; Weinberger, R. *Rosh Pinna. Sheet 2-IV. Geological Map 1:50000*; Israel Geological Survey: Jerusalem, Israel, 2016.
43. Lang, I. *Hulata, Preliminary Report*; Israel Antiquities Authority (IAA): Tel Aviv, Israel, 2022. (In Hebrew)
44. Huisman, J.A.; Hubbard, S.S.; Redman, J.D.; Annan, A.P. Measuring soil water content with ground penetrating radar: A review. *Vadose Zone J.* **2003**, *2*, 476–491. [[CrossRef](#)]
45. GPR on a Drone. Available online: <https://www.xyht.com/aerialuas/gpr-on-a-drone/> (accessed on 1 January 2023).
46. Emilsson, J.; Friborg, J.; Gustafsson, J.; Adcock, J.; Viberg, A. On the Development and Application of Airborne GPR Solutions. *First Break* **2022**, *40*, 47–54. [[CrossRef](#)]
47. Sandmeier, K.J. *REFLEXW*; Version 7.0; Windows™ 9x/NT/2000/XP/7-Program for the Processing of Seismic, Acoustic or Electromagnetic Reflection, Refraction and Transmission Data; Sandmeier Geophysical Research: Karlsruhe, Germany, 2012.

Disclaimer/Publisher's Note: The statements, opinions and data contained in all publications are solely those of the individual author(s) and contributor(s) and not of MDPI and/or the editor(s). MDPI and/or the editor(s) disclaim responsibility for any injury to people or property resulting from any ideas, methods, instructions or products referred to in the content.